Marine and Petroleum Geology 116 (2020) 104302

Contents lists available at ScienceDirect

Marine and Petroleum Geology

journal homepage: www.elsevier.com/locate/marpetgeo

Research paper

Methane hydrate-bearing sediments: Pore habit and implications

Marco Terzariol[a,1], Junghee Park[b,*], Gloria M. Castro[b], J. Carlos Santamarina[b]

[a] IFREMER, Geosciences Marines, LAD, Plouzane, France
[b] Earth Science and Engineering, Building 5, King Abdullah University of Science and Technology (KAUST), Thuwal 23955-6900, Saudi Arabia

ARTICLE INFO

Keywords:
Hydrate accumulation database
Gas production
Methane hydrate pore habit
Revised soil classification system

ABSTRACT

Hydrate-bearing sediments are relevant to the organic carbon cycle, seafloor instability, and as a potential energy resource. Sediment characteristics affect hydrate formation, gas migration and recovery strategies. We combine the physics of granular materials with robust compaction models to estimate effective stress and capillary pressure in order to anticipate the pore habit of methane hydrates as a function of the sediment characteristics and depth. Then, we compare these results to an extensive database of worldwide hydrate accumulations compiled from published studies. Results highlight the critical role of fines on sediments mechanical and flow properties, hydrate pore habit and potential production strategies. The vast majority of hydrate accumulations (92% of the sites) are found in fines-controlled sediments at a vertical effective stress between σ'_z = 400 kPa and 4 MPa, where grain-displacive hydrate pore habit prevails in the form of segregated lenses and nodules. While permeation-based gas recovery by depressurization is favored in clean-coarse sediments, gas recovery from fines-controlled sediments could benefit from enhanced transmissivity along gas-driven fractures created by thermal stimulation.

1. Introduction

Methane hydrates trap between 3×10^{15}-to-1×10^{16} m^3 of carbon in the permafrost, seafloor, and lake-bed sediments where high fluid pressures and low temperatures keep the hydrate mass stable (Boswell and Collett, 2011). The study of hydrate-bearing sediments has been driven by environmental concerns (Ruppel, 2011; Ruppel and Kessler, 2017), mechanical stability (Yun et al., 2007; Waite et al., 2009) and their resource potential (Collett, 2002; Boswell and Collett, 2006).

The sediment characteristics affect both hydrate formation as well as the selection of potential gas production strategies. In particular, hydrate pore habit depends on effective stress and pore-size-dependent capillary pressure (Booth et al., 1998; Clennell et al., 1999; Dai et al., 2012; Lei and Santamarina, 2019). The hydrate mass experiences low capillary pressure in the large pores of a clean coarse-grained sediment (without fines) as compared to the effective stress imposed by the overburden, and the growing hydrate mass readily fills pores and invades new ones without altering the sediment fabric; let's call this endmember "pore-invasive" hydrate pore habit. In contrast, "grain-displacive" hydrate pore habit takes place when high capillary pressure builds up in the small pores of fine-grained sediments and hydrate growth displaces the sediment grains to form segregated hydrate lenses and nodules.

A proper understanding of hydrate morphology and sediment characteristics will enhance the analyses of hydrate bearing sediments in view of natural and engineered processes. In this study, we develop a robust methodology to anticipate the pore habit of methane hydrates as a function of the sediment characteristics and depth. Then, we compare these results to an extensive database of worldwide sediment layers that host methane hydrates compiled from published studies.

2. Fines-controlled pore size

Pore size d_p, particle size d, specific surface S_s, and void ratio e are inter-related (Table 1Eqs. (1)–(3) – Refer to the Supplementary Material for details). The pore size d_p in clean coarse-grained sediments is a function of the grain diameter d, and ranges between $d_p = 0.15\ d$ and $d_p = 0.4\ d$ for dense and loose packings (Table 1 Eqs. (4) and (5)). On the other hand, the pore size d_p in fine sediments can be estimated from the void ratio e and specific surface S_s by assuming a parallel plate configuration: $d_p = 2e/(S_s\rho_m)$ where ρ_m is the mineral density (Table 1 Eq. (6)).

A small amount of fines can significantly alter the pore size and the sediment mechanical and fluid flow properties (see the Revised Soil

* Corresponding author.
E-mail address: junghee.park@kaust.edu.sa (J. Park).
[1] Formerly KAUST.

https://doi.org/10.1016/j.marpetgeo.2020.104302
Received 6 December 2019; Received in revised form 10 February 2020; Accepted 14 February 2020
Available online 20 February 2020

Table 1
Summary of equations required to compute the effective stress and capillary pressure profiles with depth.

Definition		Equation	Eq. #	References
Specific surface S_s	Plate-like	$S_s = \frac{area}{mass} = \frac{2L^2}{L^2 t \rho_m} = \frac{2}{t\rho_m} \rightarrow t = \frac{2}{S_s \rho_m}$	[1]	Santamarina et al. (2001)
	Sphere	$S_s = \frac{area}{mass} = \frac{4\pi r^2}{(4/3)\pi r^3} = \frac{6}{d\rho_m} \rightarrow d = \frac{6}{S_s \rho_m}$	[2]	
Void ratio e_z		$e_z = \frac{V_{void}}{V_{solid}}$	[3]	
Pore diameter d_p	Sphere (loose)	$d_p = (\sqrt{2}-1)d = \frac{6(\sqrt{2}-1)}{S_s \rho_m} \approx \frac{2.4}{S_s \rho_m}$	[4]	
	Sphere (dense)	$d_p = \left(\frac{2}{\sqrt{3}} - 1\right)d = \frac{6(2/\sqrt{3}-1)}{S_s \rho_m} \approx \frac{0.92}{S_s \rho_m}$	[5]	
	Plate-like	$d_p = e_z \cdot t = \frac{2e_z}{S_s \rho_m}$	[6]	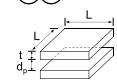
Effective stress gradient $d\sigma'_z/dz$		$\frac{d\sigma'_z}{dz} = \frac{(\rho_m - \rho_w)g}{1+e_z} = (\rho_m - \rho_w)(1-\varphi_z)g$ where $e_z = f(\sigma'_z)$	[7]	
Asymptotically-correct exponential compaction model		$e_z = e_H + (e_L - e_H)\exp\left[-\left(\frac{\sigma'_z}{\sigma'_c}\right)^{\eta}\right]$ where $\eta = 1/3$ for most marine sediments	[8]	Gregory et al. (2006), Chong and Santamarina (2016)
Effective stress σ'_z		$z = \frac{(1+e_H)}{(\rho_m - \rho_w)g}\sigma'_z + 3\frac{(e_L - e_H)}{(\rho_m - \rho_w)g}\sigma'_c\left\{\left[\left(\frac{\sigma'_z}{\sigma'_c}\right)^{\frac{2}{3}} + 2\left(\frac{\sigma'_z}{\sigma'_c}\right)^{\frac{1}{3}} + 2\right]\cdot\exp\left[-\left(\frac{\sigma'_z}{\sigma'_c}\right)^{\frac{1}{3}}\right] - 2\right\}$ for $\eta = 1/3$	[9]	
Capillary pressure $\Delta u = u_h - u_w$		$\Delta u = \frac{4T_S}{d_p}$	[10]	

Notation: L = particle length, t = particle thickness, r = radius of a sphere particle, d = particle diameter, V = volume, φ = porosity, e_L and e_H = asymptotic void ratios at low and high effective stress, σ'_c = characteristic effective stress, η = model parameter (= 1/3 in this study), g = 9.81 m/s^2, water density $\rho_w \approx 1000$ kg/m^3 and unit weight $\gamma_w = \rho_w g$, mineral density $\rho_m \approx 2650$ kg/m^3, hydrate-water interfacial tension T_s = 0.032-to-0.039 N/m.

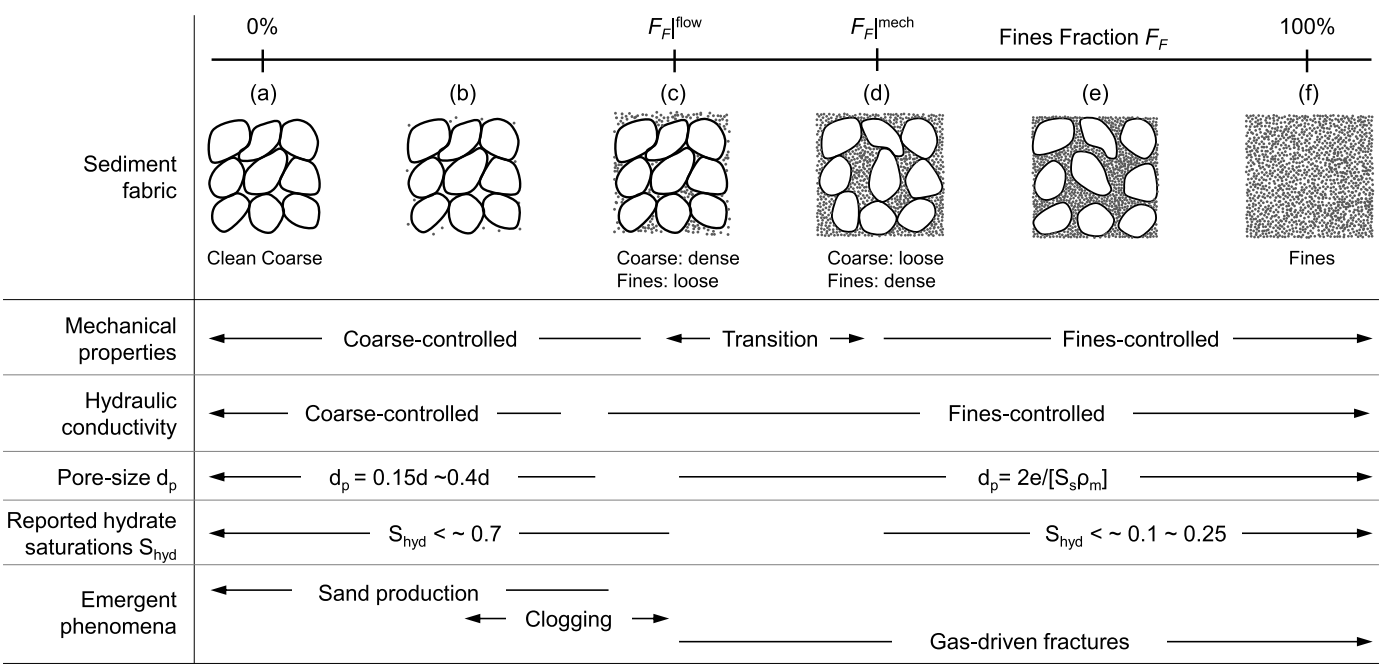

Fig. 1. The role of fines on sediment characteristics, physical properties and potential phenomena during gas production. The sketches capture critical concepts captured in the Revised Soil Classification System RSCS (Jang and Santamarina, 2016; Park and Santamarina, 2017). Note: Fines fraction $F_f = M_F/M_T$ where M_F is mass of fines and M_T is total mass of a soil mixture. $F_F|^{flow}$ indicates the threshold fines fraction for fluid flow and the $F_F|^{mech}$ indicates the threshold fines fraction for mechanical response (see details in Park and Santamarina, 2017; Park et al., 2018).

Classification System RSCS in Park and Santamarina, 2017; Park et al., 2018). Let's consider sediments as two-component mixtures (Fig. 1): coarse grains ($d > 75$-μm) and fine grains ($d \leq 75$-μm). The highest fines content $F_F|^{mech}$ at the transition from coarse-controlled to fines-controlled mechanical response corresponds to the loosely-packed coarse grains filled with densely-packed fine grains. The coarse skeleton controls mechanical properties such as strength and stiffness when $F_F < F_F|^{mech}$ (Fig. 1d). Conversely, fines form the load-carrying skeleton and control all engineering properties when coarse grains lose contact between them at $F_F > F_F|^{mech}$ and float in the fine-grained matrix thereafter (Fig. 1e). Clearly, the threshold fines fraction varies with fines plasticity, as measured by the liquid limit LL (Jang and Santamarina, 2016, 2017). For example, consider a sand with a loose-packing void ratio $e_C^{max} = 0.81$ (corresponding to a porosity $\varphi = 0.45$). The threshold fines content is: $F_F|^{mech} = 41\%$ for silt with $LL = 30$, $F_F|^{mech} = 37\%$ for kaolinite with $LL = 50$, $F_F|^{mech} = 29\%$ for illite with $LL = 120$, and $F_F|^{mech} = 19\%$ for bentonite with $LL = 300$. The threshold fines fraction for mechanical control $F_F|^{mech}$ increases as clays consolidate at higher effective stress. Therefore, we will adopt effective stress-dependent soil classification boundaries in this study.

The role of fines is even more critical on fluid transport. The threshold fines fraction for fluid flow $F_F|^{flow}$ can be estimated by the amount of fines in the form of a soft slurry needed to fill the densely-packed sand (details in Park and Santamarina, 2017). Fines control fluid flow as soon the amount of fines exceeds the threshold fines fraction for fluid flow $F_F > F_F|^{flow}$, which is lower than the threshold fines fraction for mechanical control (Fig. 1). For example, consider the same sand above: under dense packing conditions $e_C^{min} = 0.51$ (corresponding to a porosity $\varphi = 0.34$), the threshold fines contents for fluid transport are: $F_F|^{flow} = 14.1\%$ for silt with $LL = 30$, $F_F|^{flow} = 9.0\%$ for kaolinite with $LL = 50$, $F_F|^{flow} = 3.7\%$ for illite with $LL = 120$, and $F_F|^{flow} = 1.3\%$ for bentonite with $LL = 300$. Furthermore, fines can migrate and clog the coarse-grained formation even when $F_F < F_F|^{flow}$.

3. Hydrate pore habit - controls

The hydrate pore habit in natural sediments reflects the competing effects of the "compacting" vertical effective stress σ'_z and the "expanding" capillary pressure difference $\Delta u = u_h - u_w$ between the hydrate and water phases. As a first-order approximation, hydrate pore habit is pore-invasive when $\sigma'_z > \Delta u$, but is grain-displacive and forms segregated nodules and lenses when $\Delta u > \sigma'_z$ (Dai et al., 2012).

The effective stress σ'_z varies with depth z as a function of the sediment buoyant unit weight γ_{sat} - γ_w, so that $d\sigma'_z/dz = \gamma_{sat}$ - γ_w, where the saturated unit weight γ_{sat} is defined by the void ratio e_z and γ_w is the unit weight of water (Table 1 Eq. (7)). In turn, the sediment void ratio e_z depends on effective stress σ'_z. We adopt the asymptotically-correct exponential compaction model shown as Eq. (8) in Table 1 to solve the differential equation in order to determine the vertical effective stress with depth z (Table 1 Eq. (9)).

The Young-Laplace equation predicts that the capillary pressure $\Delta u = 4T_s/d_p$ is a function of the hydrate-water surface tension $T_s = 0.032$-to-0.039 N/m and the sediment pore size d_p. We use the void ratio e_z at depth z, and estimate the pore size d_p (Table 1 Eqs. (4)–(6) – Details in the Supplementary Material), and pore size d_p to compute the capillary pressure Δu with depth z (Table 1 Eq. (10)).

4. Hydrate accumulations

The physical models developed above allow us to estimate the capillary pressure Δu and effective stress σ'_z at the depth z of known hydrate accumulations to anticipate the hydrate pore habits. Table 2 summarizes published hydrate-bearing sediment data from 56 locations around the world where hydrates have been recovered or inferred from marine seismic data. We adopt the depth z^* to the Bottom Simulating Reflector BSR as the lower boundary for hydrate stability, and estimate the vertical effective stress at the BSR (Table 1 Eq. (9)). On the other hand, we assume that the representative sediment lithology for hydrate formation corresponds to the section within 50 m above the BSR. In the absence of location-specific sediment information, we extract nearby lithological information from reports produced as part of the Deep Sea Drilling Project DSDP, the Ocean Drilling Program ODP, or the International Ocean Discovery Program IODP (Note: admittedly, lack of data co-location adds uncertainty to the analyses).

Pore habit. Fig. 2a plots field cases in terms of capillary pressure Δu and effective stress at the BSR σ'_{BSR} where Δu and σ'_{BSR} are computed using equations in Table 1. Specific surface data is either published, estimated from the composition of the fines fraction, or computed from the reported liquid limit LL as S_s [m^2/g] = 1.8·LL – 34 (Santamarina et al., 2002). For reference, we superimpose trend lines for three nominal sediments using the specific surface values shown in Fig. 2b. The thick black line on Fig. 2a divides the space into two regions according to pore habit: grain-displacive when $\Delta u > \sigma'_{BSR}$ and pore-invasive when $\Delta u < \sigma'_{BSR}$. Available information (21 out of the 56 sites) suggest that most hydrate occurrences fall within the grain-displacive pore habit regime (19 out of 21 sites).

For example, the reported specific surfaces are $S_S = 87$–94 m^2/g for KGB #32 and $S_S = 21$–110 m^2/g for ULB #50; as expected, these two sites fall between the trend lines for $S_S = 10$ m^2/g and $S_S = 100$ m^2/g (Fig. 2a). Specific surface values estimated from the reported liquid limits are in agreement with trend lines as well; examples include: $S_S = 115$ m^2/g for BOR #7, $S_S = 126$ m^2/g for NOR #15, $S_S = 38$ m^2/g for BAS #18, $S_S = 105$ m^2/g for GOM #30, $S_S = 101$ m^2/g for GUA #38, $S_S = 81$–120 m^2/g for HYR #40, and $S_S = 65$ m^2/g for BAL #52. These results confirm that well tested correlations between index properties can be most valuable to assess hydrate pore habits.

Fines-controlled flow and mechanical response. The middle panel, Fig. 2c, plots the fines content for the 56 hydrate accumulations versus the effective stress σ'_{BSR} at the BSR. The computed thresholds for flow-control $F_F|^{flow}$ and mechanical-control $F_F|^{mech}$ correspond to the three types of fines listed in Fig. 2b (Input parameters in Table 3). These boundaries capture the controlling role of fines on the mechanical and fluid flow properties as a function of effective stress and specific surface. Based on the available information, we can classify 46 out of the 56 sites using these boundaries: 2 sites have coarse-controlled properties, 2 sites fall in the transitional regime, and 42 of the 46 sites exhibit fines-controlled mechanical and flow properties (Fig. 2c and d).

Coarse-controlled sites benefit from high permeability (gas recovery) and mechanical stability (simpler well completion – see Shin and Santamarina, 2017). Note that Mt. Elbert #24 has a similar fines content as Okushiri Ridge #49 and both will exhibit fines-controlled permeability and mechanical response; yet Mt. Elbert #24 is at high effective stress and the hydrate is pore-invasive, while segregated nodules dominate the shallow accumulation at Okushiri Ridge #49.

Fig. 2e provides a statistical summary of the field conditions at

Table 2
Methane hydrate accumulations around the world.

Water body	Designation	#	Location	Water depth to seafloor [mbsl]	Depth to base of MHBZ [mbsf]	Maximum effective stress [kPa]	Hydrate pore habit	Sediment description
Antartic	RSS	1	Ross Sea	950 (ci)	380 (ci)	1900		Clay = 59%; Silt = 40%; Sand = 1% (cj)
	WDS	2	Weddel Sea	1300 (cf)	335 (cf)	1650		Clay = 40%; Silt = 50%; Sand = 10% (cg)
	WLM	3	Wilkes Land Margin	980 (ch)	500 (ch)	2500		ND
Atlantic ocean	AMA	4	Amazon Fan	1000-3000 (p,q)	360 (p)	1800		Clay = 13%; Silt = 85%; Sand = 0.15% (ba)
	AMV	5	El Arraiche Mud Volcano Field	380-900 (dg,dh)	0-75 (dg)	375	Nodules (di)	Mud breccia (clay; dk)
	AR	6	Malvinas Basin	500-5000 (i)	50 (i)	250		Olive green mud (ay)
	BOR/BR	7	Blake Ridge & Outer Ridge	3000-3600 (a)	450-600 (a,c)	3000	Nodules (e)	Clay = 70–86%; Silt = 11–28%; Sand = 0.3–3%; Liquid limit LL = 83 (b,u,d,aw,e,av,ax)
	BRA	8	Pelotas Basin	500 to 3000 (o)	300 (o)	1500		ND
	CAR	9	Carolina Trough	800-2200 (bg)	300 (bg)	1500	Nodules (bm)	Clay = 85%; Silt = 15%; Sand = 0% (bh)
	COG	10	Congo-Angola Margin	600-3000 (db,dc)	0-190 (dc)	0–950	Nodules (db)	Clay = 25–75%; Silt = 25–75%; Sand = 0% (dd); Mostly kaolinite and quartz (db)
	CON	11	Continental Rise	2700 to 3400 (s)	400 (s)	2000		Clay = 75%; Sand-silt = 25% (t)
	NAB	12	Namibe Basin	1000 (dl)	250 (dl)	1250	Nodules (dl)	Diatom bearing clay; Clay = 30–60%; Silt = 5–10%; Sand = 0% (dm)
	NDF	13	Niger Delta Front	2400-2900 (cy,cz)	300-380 (cy)	1800	Nodules/lenses (cz)	Fines = 80%; Sand = 20% (da)
	NFL	14	Newfoundland	620-2850 (ee)	251-443 (ee)	2215		ND
	NOR	15	Continental Slope	1500 (x)	150 (w)	750	Nodules (dj)	Clay = 54%; Silt = 45%; Sand = 1%; LL = 89–105; PL = 55–69 (y)
	URU	16	Punta del Este Basin	350 to 2200 (m)	400 (m)	2000		ND
Artic & Nearby	ALT	17	Aleutian Trench	2110 (bn)	670 (bn)	3350		Clay = 45%; Silt = 25%; Spicules = 5%; Diatoms = 25% (ao)
	BAS	18	Barents Sea	345 (bq)	180 (bq)	900		Clay = 60%; Silt = 20%; Sand = 20%; LL = 40 (br)
	BES	19	Beaufort Sea	50-200 (dv)	800-1500 (dv)	7500		Silt and Clay = 60–70%; Sand = 30–40% (dv)
	FMS	20	Fram Strait	1700-2500 (bs)	200 (bs)	1000		Clay = 65%; Silt = 30%; Sand = 5% (bt)
	KRY	21	Shirshov Ridge/Koryak	1500-3000 (de)	200-500 (de)	2500		Clay = 5.6–12.1%; Silt = 11.3–25.8%; Sand = 62.1–83.1% (df)
	LTB	22	Lena-Tunguska Basin	N/A	800-2000 (bo)	10,000		ND
	MAL	23	Mallik (Canada)	N/A	1000 (bl)	5000	Pore filling (bl)	Fine/medium sand, Mean grain size D_{50} = 149.9–502.5 μm (bl,ec)
	MEL	24	Mt Elbert	N/A	850 (bi)	4250	Pore filling (bj)	Passing sieve No. 200 = 56–61%; D_{50} = 0.07–0.074 mm (bi,bk)
	SOO	25	Sea of Okhotsk	500-1500 (cr)	50-800 (cr)	4000	Nodules (ct), lenses (cu)	Clay = 20.4–26.3%; Silt = 73–79%; Sand = 0–5% (cv)
	SVE	26	Sverdrup Basin	N/A	900 (bo,bb)	4500		Sandstone (eg)
	WSB	27	West Siberia Basin	N/A	800 (bp)	4000		0.2 mm = 8%; 0.5 mm = 4%; 0.8 mm = 4%; > 1 mm = 84% (bp)
Caribbean	BAR	28	Barbados Ridge	3300-5000 (be)	750 (be)	3750		Clay = 78%; Silt = 20%; Sand = 2% (bf)
	COB	29	Colombia Basin	2100 (r)	300 (r)	1500		Mostly nannofossils and clay; Clay = 25–75% (v,az)
	GOM	30	Gulf of Mexico (*)	440-2400 (ca)	Surface-300 (cc)	0–1500	Nodules (ca)	Clay = 50–80%; Silt = 20–50%; Sand = 0–1% (ca,ce); LL = 51.2–77; PL = 20.7–30.5 (cd)
Indian	GOO	31	Gulf of Oman	3000 (cw)	670-690 (cw)	3500		Clay = 64–76%; Silt = 24–36%; Sand = 0% (cx)
	KGB	32	Krishna-Godavari Basin	895-2663 (bw)	120-608 (bw)	3000	Nodules/Lenses (bv)	Clay = 50–70%; Silt = 30–50%; S_S = 87–94 m^2/g; LL = 73–75; PL = 34–36 (bu)
	SUA	33	Sunda Arc	1500-2200 (dw)	150 (dw)	750		ND
Pacific	ACA	34	Acapulco	2000-3800 (a)	380 (a)	1900	Nodules (as)	Clay = 30%; Silt = 50%; Sand = 20% (as)
	COP	35	Pacific	900-3100 (ai)	300 (ai)	1500		ND
	CTJ	36	Chile Triple Junction region	2200-2700 (ap)	100 (ap)	1250		Clay = 49%; Silt = 44%; Sand = 7% (ar,bb)
	ERB	37	Eel River Basin	800-2000 (ae,af)	225-315 (ae)	1500	Nodules (ae)	Turbidites; Clay = 64%; Silt = 35%; Sand = 1% (ag,ah)
	GUA	38	Guatemala/Costa Rica/ Nicaragua	1000-1300 (a)	200-500 (a)	1500	Nodules (f)	Clay = 63%; Silt = 30%; Sand = 7%; LL = 75–120; Plastic index PI = 35–75 (g)
	HIK	39	Hikurangi	3530 (at)	160 (at)	800	Lenses (au)	Clay = 58%; Silt = 40%; Sand = 2% (du)
	HYR	40	Hydrate Ridge	890 (j)	125 (j)	625	Layered (j)	Clay = 50%; Silt = 50%; LL = 64–86; Plastic limit PL = 35–40 (j)
	KAC	41	Kaoping Canyon	900-1700 (dx)	200 (dx)	1000		ND
	LHR	42	Tasman Sea/Lord Howe Rise	3600 (dq)	520-600 (dq)	3000		Clay > 75%; Silt = 5–25% (dr)
	LIB	43	Lima Basin	1000-6000 (bc)	470-610 (bc)	2500	Nodules (bc)	Diatomaceous mud; Clay = 55%; Silt = 45% (bd)

(*continued on next page*)

Table 2 (*continued*)

Water body	Designation	#	Location	Water depth to seafloor	Depth to base of MHBZ	Maximum effective stress	Hydrate pore habit	Sediment description
				[mbsl]	[mbsf]	[kPa]		
	NT	44	Nankai Trough	950 (aj)	250 (aj)	1250	Pore filling (aj)	Clay = 1–3%; Silt = 26–36%; Sand = 61–72% (ak) LL = 68 (ec)
	NCM	45	Northern Cascadia Margin	950-1850 (ab)	150 (ab)	750	Nodules and pore filling (ad)	Clayey silt; D_{50} = 7–16 μm (ac)
	PAN	46	Panama	1800-2800 (a)	180-300 (a)	1500		Clay = 70%; Silt = 28%; Sand = 2% (h)
	SCM	47	Southern Cascadia Margin	800-2000 (an)	65-125 (an)	625	Nodules (al)	Clay = 40–70%; Silt = 30–50%; Sand = 0–4% (am)
	SHA	48	Shenhu Area	1500 (l)	240 (l)	1200	Pore filling (dt); Nodules (dz)	Clay = 25%; Silt = 70%; Sand = 5% (k)
Sea of Japan/East Sea	OKR	49	Okushiri Ridge	2500 (bl)	90 (bl)	450	Nodules (bz)	Clay = 35% Silt = 25% Sand = 40% (ed) LL = 113–143 (ec)
	ULB	50	Ulleung Basin	2100 (bx,by)	150 (by)	750	Nodules/Lenses (by)	Passing sieve No. 200 = 100%; D_{50} = 2.27–3.04 μm; S_S = 20.9–110.7 m^2/g (bx)
Others	ANM	51	Anaximander Mud Volcanoes	2025 (ds)	40-200 (ds)	1000	Nodules (ds)	Clay = 56–67%; Silt = 19–30%; Sand = 14% (ds)
	BAL	52	Baikal Lake	1600 (ck)	160 (ck)	0–800	Nodules and lenses (ck)	Clay = 70%; Silt = 5%; Sand = 25%; LL = 55–100 (cl)
	BLS	53	Black sea	1500-2000 (co)	350 (co)	1750	Nodules and lenses (cp)	Particle diameter d < 0.01 mm = 70–90%; 0.1 > d > 0.01 mm = 10–30%; d > 0.1 mm = 0% (cq)
	CAS	54	Caspian Sea	475-600 (cm)	400 (cn)	0–2000	Nodules and lenses (cm)	Pass sieve No. 200 = 97% (cm)
	QMT	55	Qilian Mountains Tibet	N/A	133-396 (dy)	600–2000	Fracture filling in rock (dy, eb)	Medium-sized sandstone, fine sandstone, siltstone, clayey siltstone, mudstone and oil shale (ea)
	WMS	56	Western Marmara Sea	680 (dn,do)	25-100 (dn,do)	500	Nodules (do)	Clay = 50–70%; Silt = 30–40%; Sand = 0–1% (dp)

(*) for the purpose of this study, 'Gulf of Mexico' includes: East Breaks, Keathley Canyon, Garden Banks, Green Canyon, Walker Ridge and Mississippi Canyon.
Note: N/A = not applicable; ND = No data available or incomplete information to infer soil type.
References: (a) Shipley et al., (1979); (b) Boyce (1973); (c) Kvenvolden and Barnard (1983); (d) Collett and Wendlandt (2000); (e) Matsumoto et al. (2000); (f) Kvenvolden and McDonald (1985); (g) Taylor and Bryant (1985); (h) Boyce (1972); (i) Manley and Flood (1989); (j) Tan et al. (2006); (k) Wang et al. (2011); (l) Wang et al. (2018); (m) Santa Ana et al. (2008); (n) Tomasini et al. (2011); (o) Oliveira et al. (2010); (p) Manley and Flood (1988); (q) Piper et al. (1997); (r) Reed et al. (1990); (s) Tucholke et al. (1977); (t) Hollister and Shipboard Scientific Party (1972); (u) Sheridan and Shipboard Scientific Party (1980); (v) Warren and Shipboard Scientific Party (1979); (w) Kvenvolden et al. (1989); (x) Talwani and Shipboard Scientific Party (1976); (y) Pittinger (1989); Winters (2000); (aa) Collett and Ladd (2000); (ab) Westbrook and Shipboard Scientific Party (1994a); (ac) Westbrook and Shipboard Scientific Party (1994b); (ad) Expedition 311 Scientists (2005); (ae) Brooks et al. (1991); (af) McManus and Shipboard Scientific Party (1969a); (ag) Vallier (1969); (ah) McManus and Shipboard Scientific Party (1969b); (ai) Minshull et al. (1994); (aj) Uchida et al. (2004); (ak) Yoneda et al. (2015); (al) Hovland et al. (1995); (am) Camerlenghi et al. (1995); (an) Carson et al. (1995); (ao) Creager and Shipboard Scientific Party (1973b); (ap) Bangs et al. (1995); (aq) Brown et al. (1996); (ar) Behrmann and Shipboard Scientific Party (1992); (as) Moore and Shipboard Scientific Party 1982(); (at) Pecher et al. (2018); (au) Schwalenberg et al. (2010); (av) Paull and Shipboard Scientific Party (1996a); (aw) Paull and Shipboard Scientific Party (1996b); (ax) Paull and Shipboard Scientific Party (1996c); (ay) von Lom-Keil et al., 2002; (az) Mayer, 1982; (ba) Manley et al. (1997); (bb) Majorowicz et al. (2002); (bc) Kvenvolden and Kastner (1990); (bd) Suess and Shipboard Scientific Party (1990); (be) Ladd et al. (1981); (bf) Biju-Duval and Shipboard Scientific Party (1984); (bg) Dillon et al. (1982); (bh) Paull and Shipboard Scientific Party (1996d); (bi) Dai et al. (2011); (bj) Dai et al. (2012); (bk) Winters et al. (2011); (bl) Uchida et al. (2000); (bm) Uchida et al. (1997); (bn) Shipboard Scientific Party (1973); (bo) Collett and Dallimore (2000); (bp) Collett and Ginsburg (1998); (bq) Andreassen et al. (1990); (br) Sættem et al. (1992); (bs) Hustoft et al. (2009); (bt) Jansen and Shipboard Scientific Party (1996); (bu) Yun et al. (2010); (bv) Winters et al. (2008); (bw) Collett et al. (2008); (bx) Lee et al. (2011); (by) Kim et al. (2011); (bz) Tamaki et al. (1990); (ca) Pflaum et al. (1986); (cb) Bouma et al. (1986); (cc) Boswell et al. (2009); (cd) Yun et al. (2006); (ce) Sawyer et al. (2009); (cf) Lonsdale (1990); (cg) Barker and Shipboard Scientific Party (1988); (ch) Kvenvolden et al. (1987); (ci) Geletti and Busetti (2011); (cj) Hayes and Shipboard Scientific Party (1975); (ck) Khlystov et al. (2013); (cl) Kataoka et al. (2009); (cm) Ginsburg et al. (1992); (cn) Diaconescu and Knapp (2002); (co) Popescu et al. (2006); (cp) Akhmetzhanov et al. (2007); (cq) Trimonis and Shimkus (1978); (cr) Lüdmann and Wong (2003); (cs) Parlaktuna and Erdogmus (2001); (ct) Shoji et al. (2005); (cu) Luan et al. (2008); (cv) Dang et al. (2010); (cw) White (1979); (cx) Whitmarsh and Shipboard Scientific Party (1974); (cy) Hovland et al. (1997); (cz) Wei et al. (2015): (da) Sultan et al. (2016); (db) Charlou et al. (2004); (dc) Gay et al. (2007); (dd) Wefer and Shipboard Scientific Party (1998a); (de) Cooper et al. (1987); (df) Bode (1973); (dg) Depreiter et al. (2005); (dh) Gardner (2001); (di) Mazurenko et al. (2002); (dj) Ginsburg et al. (1999); (dk) Kenyon et al. (2000); (dl) Swart (2009); (dm) Wefer and Shipboard Scientific Party (1998b); (dn) Sarıtaş et al. (2018); (do) Bourry et al. (2009); (dp) Bodur and Ergin (1994); (dq) Exon et al. (1998); (dr) Kennet and Shipboard Scientific Party (1986); (ds) Lykousis et al. (2009); (dt) Wang et al. (2014b); (du) Carter and Shipboard Scientific Party (2000); (dv) Weaver and Stewart (1982); (dw) Kopp (2002); (dx) Lin et al. (2009); (dy) Zhao et al. (2013); (dz) Liu et al., (2015); (ea) Lu et al. (2011); (eb) Wang et al. (2014a); (ec) Dai et al. (2012); (ed) Tamaki and Shipboard Scientific Party (1990); (ee) Mosher (2011); (ef) Baristeas et al. (2012); (eg) Judge et al. (1994).

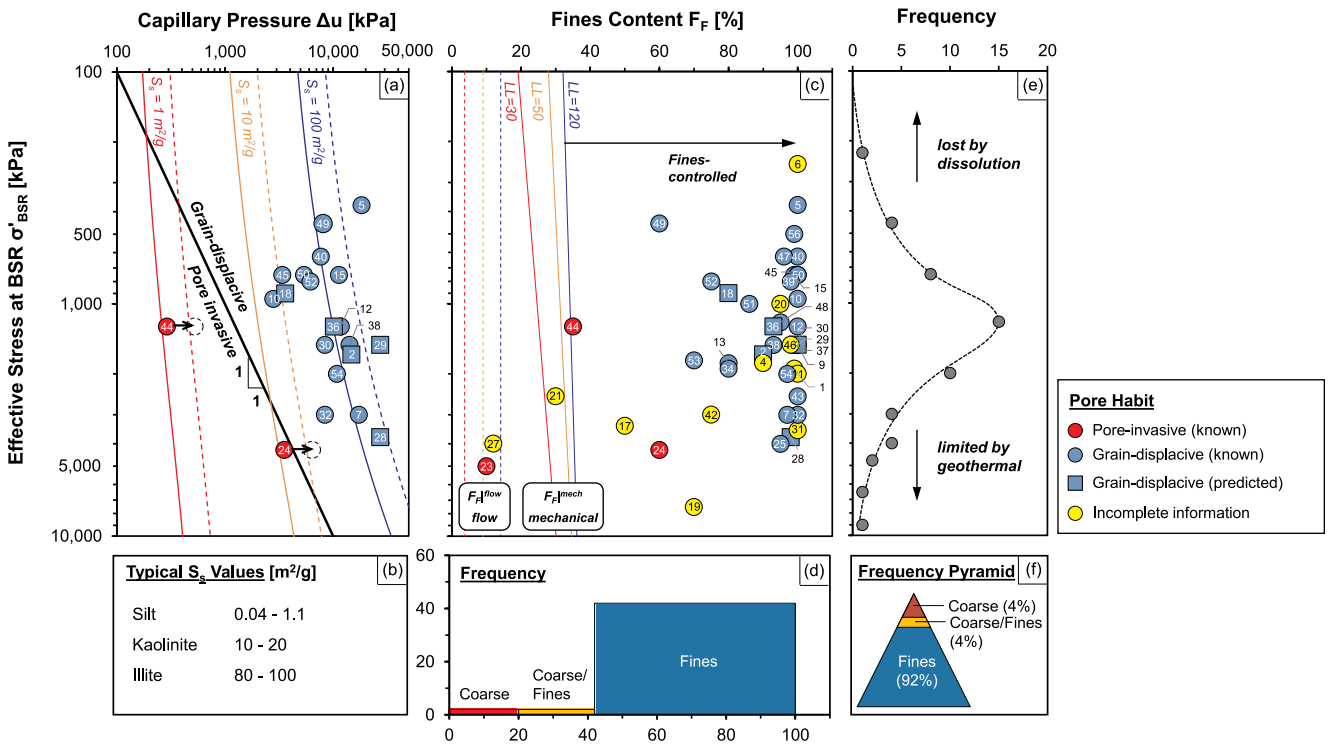

Fig. 2. Hydrate bearing sediments – Worldwide accumulations (56 sites). (a) Pore habit as a function of capillary pressure and effective stress at the BSR. (b) Specific surface values for different fine sediments. (c) Fines content for 46 sites and classification boundaries - dotted lines: threshold fines fraction for fluid transport $F_F|^{flow}$; continuous lines: threshold fines fraction for mechanical response $F_F|^{mech}$ (Note: input parameters in Table 3). (d) Hydrate accumulation histograms according to sediment type, (e) Hydrate accumulation histograms according to effective stress at the BSR. (f) Frequency pyramid.

hydrate accumulation sites: most accumulations exist at 400 kPa < σ'_{BSR} < 4 MPa. The vertical axis in Fig. 2e is the expected maximum effective stress at the BSR. This histogram shows the reduced probability of hydrate accumulations near the seafloor under diffusion-limited conditions; on the other hand, the geothermal gradient limits accumulations at depth. Finally, the resource pyramid in Fig. 2f highlights the fact that fines-controlled sediments host most hydrate accumulations (92% of known sites).

Global distribution. The world map in Fig. 3 shows the methane hydrate accumulations compiled for this study. The color coding captures the pore habit: red for the 3 locations with known pore-invasive morphology, blue for the 32 locations with grain-displacive fines-controlled accumulations (circle: 27 known pore habit; square: 5 predicted pore habit), and green for the 21 sites with incomplete information (i.e., missing pore habit, specific surface, liquid limit or pore size distribution - Note: QMT #55 exhibits fracture-filling hydrate in rocks). Coarse-dominant hydrate-bearing sediments are reported at three locations only: the Nankai Trough, the Arctic and Antarctica.

Table 3
Input parameters for the estimation of threshold fines fractions for fluid flow and mechanical control.

Coarse		Fines				Threshold fines fraction	
Void ratio		Liquid limit LL	Specific surface S_s [m²/g]	Void ratio		Fluid flow $F_F\|^{flow}$ [%]	Mechanics $F_F\|^{mech}$ [%]
Minimum void ratio e_C^{min}	0.51	Silt	0.04–1.1	$e_F\|^{flow}$	2.10	14.1	–
		LL = 30		$e_F\|^{100kPa}$	0.71	–	32.1
				$e_F\|^{1MPa}$	0.54	–	34.5
				$e_F\|^{10MPa}$	0.43	–	36.2
		Kaolinite	10–20	$e_F\|^{flow}$	4.13	9.0	–
		LL = 50		$e_F\|^{100kPa}$	1.09	–	27.9
Maximum void ratio e_C^{max}	0.81			$e_F\|^{1MPa}$	0.76	–	31.5
				$e_F\|^{10MPa}$	0.53	–	34.6
		Illite	80–100	$e_F\|^{flow}$	12.4	3.7	–
		LL = 120		$e_F\|^{100kPa}$	2.42	–	19.1
				$e_F\|^{1MPa}$	1.53	–	24.3
				$e_F\|^{10MPa}$	0.88	–	30.1

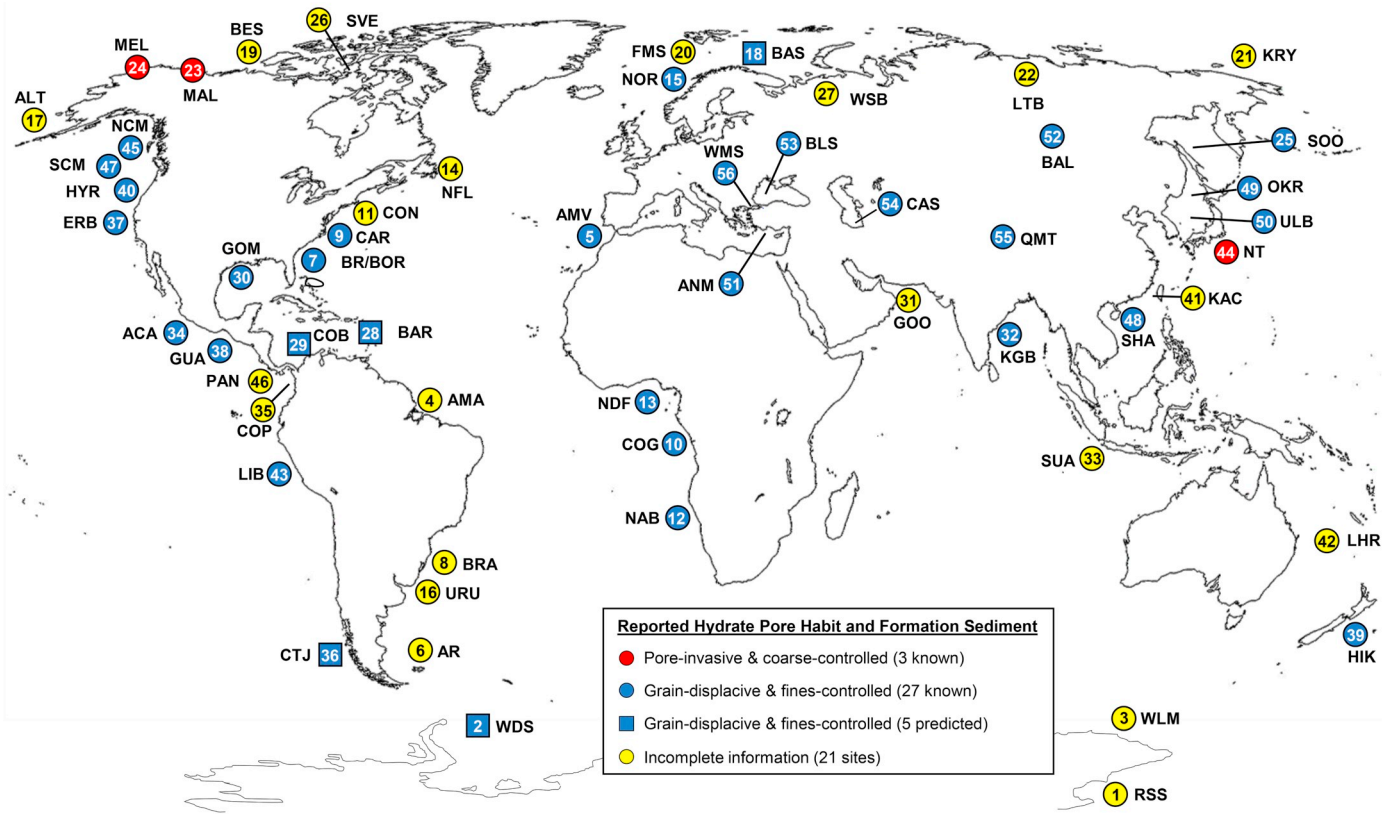

Fig. 3. Methane hydrate-bearing sediments around the world. Hydrate pore habit and formation characteristics. GOM #30: hydrates reported near surface and at depth. NCM #45: has been reported as both grain-displacive and pore-invasive.

5. Discussion: gas production

Pore-invasive methane hydrate accumulations in highly-permeable and mechanically-stable coarse sediments are the most desirable reservoir characteristics for depressurization-driven gas production strategies (Moridis et al. 2007, 2011a). For example, hydrate dissociation in the Nankai Trough #44 falls below the boundary in the capillary pressure vs. effective stress map, and gas will flow through the connected pores (Note that fines may migrate and potentially clog the pores in the coarse fraction).

Once the hydrate dissociates, gas permeates through the sediment pores if the capillary pressure is lower than the effective stress (Sun and Santamarina, 2019). Gas permeation boundaries are parallel to the hydrate morphology boundaries (dotted lines in Fig. 2a), but shifted to the right to take into consideration the higher interfacial tension in gas-water $T_s \approx 0.072$ N/m compared to hydrate-water $T_s \approx 0.040$ N/m.

Depressurization-driven gas production from coarse-dominant sediments may cause sand production (see Fig. 1), and affect the operation of wells, as experienced in Mallik (Canada in 2007 - Dallimore et al., 2012) and Nankai Trough (Japan in 2013 - Yamamoto et al., 2014).

On the other hand, high depressurization will be required to extract gas from sediments with fines-controlled fluid flow. In turn, this will cause an increase in effective stress, sediment compaction (will require special well completion designs to avoid buckling collapse – Moridis et al., 2011b; Shin and Santamarina, 2017), reduced permeability (Chapuis, 2012; Ren and Santamarina, 2018), and faster pressure recovery radially away from the well leading to smaller producible volume (Tabatabaie and Pooladi-Darvish, 2009; Wang et al., 2015; Terzariol et al., 2017).

Alternatively, the large volume expansion during hydrate dissociation can be used in heating-based production strategies to cause gas-driven fractures within fines-controlled formations. Note that thermal dissociation may trigger gas-driven fracture formation even when hydrate formation was pore-invasive (e.g., Mt. Elbert #24). Once again, the reservoir will experience large deformations and will require proper well design. Furthermore, thermal stimulation is energy intensive: most of the injected heat is taken by the sediments (mineral and water) and spreads unconstrained by bounding aquitards (Moridis et al., 2007; Moridis, 2008). Therefore, the viability of thermal stimulation improves for accumulations near the phase boundary, i.e., near the BSR.

6. Conclusions

Sediments control hydrate accumulation, pore habit, spatial distribution and potential gas production strategies. Hydrate pore habit depends on sediment type and depth-dependent capillary pressure and effective stress. A similar analysis and parameters used for hydrate formation define gas permeation boundaries as well. Results highlight the critical role of fines and implications on gas migration and potential production strategies. Threshold fines fractions identified for mechanical- and flow-controls properly guide the analyses of hydrate pore habit.

The vast majority of hydrate accumulation sites (92% of the sites) are found in fines-controlled sediments at a vertical effective stress between $\sigma'_z = 400$ kPa and 4 MPa, where grain-displacive hydrate pore habit prevails in the form of segregated lenses and nodules.

Permeation-based gas recovery by depressurization is favored in clean coarse sediments. Gas production from hydrates in fines-controlled sediments could benefit from enhanced-gas transmissivity along gas-driven fractures created by thermal stimulation; the viability of energy-intensive thermal stimulation improves for accumulations near the BSR.

Data availability

All data used in this study are stored in the Figshare, located at: https://doi.org/10.6084/m9.figshare.11294249.

Declaration of competing interest

The authors declare that they have no known competing financial interests or personal relationships that could have appeared to influence the work reported in this paper.

Acknowledgments

Support for this research was provided by the KAUST Endowment at King Abdullah University of Science and Technology. This study was conducted by the authors at KAUST. Gabrielle E. Abelskamp edited the manuscript.

Appendix A. Supplementary data

Supplementary data to this article can be found online at https://doi.org/10.1016/j.marpetgeo.2020.104302.

List of notations

D_{50}	mean grain size
d	grain diameter
d_p	pore size
e	void ratio (Subscripts: L = at $\sigma'_z \rightarrow 0$, H = at $\sigma'_z \rightarrow \infty$, z = at depth z)
e_C^{min}	minimum void ratio (coarse grain sediment packed at maximum density)
e_C^{max}	maximum void ratio (coarse grain sediment in loosest state)
F_F	fines fraction
$F_F\|^{flow}$	threshold fines fraction for fluid flow
$F_F\|^{mech}$	threshold fines fraction for mechanical response
g	gravity (g = 9.81 m/s^2)
L	length and width of plate-like particle
LL	liquid limit
M	mass (Subscripts: F = fines, T = total)
PL	plastic limit
r	radius of a spherical particle
S_{hyd}	hydrate saturation
S_s	specific surface
T_s	hydrate-water surface tension
t	thickness of plate-like particle
u	pressure (Subscripts: h = hydrate phase, w = water phase)
Δu	capillary pressure = difference between the hydrate and water phases
V	volume
z	depth from the seafloor
z^*	depth from the seafloor to BSR
γ	unit weight (Subscripts: sat = saturated sediment, w = water)
η	compaction model parameter
ρ	mass density (Subscripts: m = mineral, w = water)
σ'_{BSR}	effective stress at the BSR
σ'_c	characteristic effective stress
σ'_z	vertical effective stress at depth z from the seafloor
φ	porosity

References

Akhmetzhanov, A.M., Ivanov, M.K., Kenyon, N.H., Mazzini, A., 2007. Deep-water Cold Seeps, Sedimentary Environments and Ecosystems of the Black and Tyrrhenian Seas and the Gulf of Cadiz. United Nations Educational, Scientific and Cultural Organisation (UNESCO).
Andreassen, K., Hogstad, K., Berteussen, K.A., 1990. Gas hydrate in the southern Barents Sea, indicated by a shallow seismic anomaly. First Break 8 (6), 235–245.
Bangs, N.L.B., Sawyer, D.S., Golovchenko, X., 1995. The cause of the bottom-simulating reflection in the vicinity of the Chile Triple Junction. In: Proceedings of the Ocean Drilling Program. Scientific Results. vol. 141. pp. 243–252.
Baristeas, N., Anka, Z., Di Primio, R., Rodriguez, J.F., Marchal, D., Dominguez, F., 2012. Distribution of hydrocarbon leakage indicators in the Malvinas Basin, offshore Argentine continental margin. Mar. Geol. 332, 56–74.
Barker, Shipboard Scientific Party, 1988. Site 695. In: Proceedings of the Ocean Drilling Program, vol. 113. pp. 527–606 Initial Reports.
Behrmann, J.H., Shipboard Scientific Party, 1992. Site 860. In: Proceedings of the Ocean Drilling Program, vol. 141. pp. 159–238 Initial Reports.
Biju-Duval, B., Shipboard Scientific Party, 1984. Site 541: toe of the Barbados ridge complex. In: Proceedings of the Deep Sea Drilling Project, vol. 78. pp. 107–186 Initial Reports.
Bode, G.W., 1973. Grain size. In: Proceedings of the Deep Sea Drilling Project, vol. 19. pp. 661–662 Initial Reports.
Bodur, M.N., Ergin, M., 1994. Geochemical characteristics of the recent sediments from the Sea of Marmara. Chem. Geol. 115 (1–2), 73–101.
Booth, J.S., Winters, W.J., Dillon, W.P., Clennell, M.B., Rowe, M.M., 1998. Major occurrences and reservoir concepts of marine clathrate hydrates: implications of field evidence. Geol. Soc. Lond. Special Pub. 137 (1), 113–127.
Boswell, R., Collett, T., 2006. The gas hydrates resource pyramid. Fire in the Ice. pp. 1–4.
Boswell, R., Shelander, D., Lee, M., Latham, T., Collett, T., Guerin, G., Moridis, G., Reagan, M., Goldberg, D., 2009. Occurrence of gas hydrate in oligocene frio sand: alaminos Canyon block 818: northern gulf of Mexico. Mar. Petrol. Geol. 26 (8), 1499–1512.
Boswell, R., Collett, T.S., 2011. Current perspectives on gas hydrate resources. Energy Environ. Sci. 4 (4), 1206–1215.
Bouma, A.H., Coleman, J.M., Meyer, A.W., 1986. Introduction, objectives, and principal results of Deep Sea drilling project leg 96. Initial Reports of the Deep Sea Drilling Project. 96. pp. 15–36.
Bourry, C., Chazallon, B., Charlou, J.L., Donval, J.P., Ruffine, L., Henry, P., Geli, L., Çagatay, M.N., İnan, S., Moreau, M., 2009. Free gas and gas hydrates from the Sea of Marmara, Turkey: chemical and structural characterization. Chem. Geol. 264 (1–4), 197–206.
Boyce, R.E., 1972. Grain size analyses Leg 9. Proc. Deep Sea Drill. Project 9, 779–796 Initial Reports.
Boyce, R.E., 1973. Leg 11 grain size analysis. Proc. Deep Sea Drill. Project 11, 1047–1057 Initial Reports.
Brooks, J.M., Field, M.E., Kennicutt II, M.C., 1991. Observations of gas hydrates in marine sediments, offshore northern California. Mar. Geol. 96 (1–2), 103–109.
Brown, K.M., Bangs, N.L., Froelich, P.N., Kvenvolden, K.A., 1996. The nature, distribution, and origin of gas hydrate in the Chile Triple Junction region. Earth Planet Sci. Lett. 139 (3–4), 471–483.
Camerlenghi, A., Lucchi, R.G., Rothwell, R.G., 1995. Grain-size analysis and distribution in Cascadia Margin sediments, northeastern Pacific. In: Proceedings of the Ocean Drilling Program, Scientific Results, vol. 146. pp. 3–32.
Carson, B., Westbrook, G.K., Musgrave, B., 1995. Ocean Drilling program, leg 146 preliminary report, cascadia margin. In: Proceedings of the Ocean Drilling Program, pp. 146 Initial Reports.
Carter, Shipboard Scientific Party, 2000. Leg 181 preliminary report – southwest pacific gateways – site 1124. In: Proceedings of the Ocean Drilling Programpp. 181 Initial Reports.
Chapuis, R.P., 2012. Predicting the saturated hydraulic conductivity of soils: a review. Bull. Eng. Geol. Environ. 71 (3), 401–434.
Charlou, J.L., Donval, J.P., Fouquet, Y., Ondreas, H., Knoery, J., Cochonat, P., Levaché, D., Poirier, Y., Jean-Baptiste, P., Fourré, E., Chazallon, B., 2004. Physical and chemical characterization of gas hydrates and associated methane plumes in the Congo–Angola Basin. Chem. Geol. **205** (3–4), 405–425.
Chong, S.H., Santamarina, J.C., 2016. Soil compressibility models for a wide stress range. J. Geotech. Geoenviron. Eng. 142 (6).
Clennell, M.B., Hovland, M., Booth, J.S., Henry, P., Winters, W.J., 1999. Formation of natural gas hydrates in marine sediments: 1. Conceptual model of gas hydrate growth conditioned by host sediment properties. J. Geophys. Res.: Solid Earth 104 (B10), 22985–23003.
Collett, T.S., 2002. Energy resource potential of natural gas hydrates. AAPG Bull. 86 (11), 1971–1992.
Collett, T.S., Ginsburg, G.D., 1998. Gas hydrates in the Messoyakha gas field of the West Siberian Basin - a re-examination of the geologic evidence. Int. J. Offshore Polar Eng. 8 (1).
Collett, T.S., Ladd, J., 2000. 19. Detection of gas hydrate with downhole logs and assessment of gas hydrate concentrations (saturations) and gas volumes on the Blake Ridge with electrically resistivity log data. In: Proceedings of the Ocean Drilling Program, Scientific Results, vol. 164. pp. 179–191.
Collett, T.S., Wendlandt, R.F., 2000. Formation evaluation of gas hydrate-bearing marine sediments on the Blake Ridge with downhole geochemical log measurements. In: Proceedings of the Ocean Drilling Program, Scientific Results, vol. 164. pp. 199–215.
Collett, T.S., Dallimore, S.R., 2000. Permafrost-associated gas hydrate. In: Natural Gas Hydrate. Springer, Dordrecht, pp. 43–60.
Collett, T.S., Riedel, M., Cochran, J.R., Boswell, R., Kumar, P., Sathe, A.V., 2008. July). Indian continental margin gas hydrate prospects: results of the Indian National Gas Hydrate Program (NGHP) expedition 01. In: Proceedings of the 6th International Conference on Gas Hydrates, (Vancouver, Canada).
Cooper, A.K., Scholl, D.W., Marlow, M.S., 1987. Structural Framework, Sedimentary

Sequences, and Hydrocarbon Potential of the Aleutian and Bowers Basins, Bering Sea. *Geology And Resource Potential Of the Western*, vol. 6 North America and Adjacent Ocean Basins–Beaufort Sea to Baja California.
Creager, J.S., Shipboard Scientific Party, 1973b. Site 185. In: Proceedings of the Deep Sea Drilling Project, Initial Reports, vol. 19. pp. 169–216.
Dai, S., Lee, C., Santamarina, J.C., 2011. Formation history and physical properties of sediments from the Mount Elbert gas hydrate stratigraphic test well, Alaska North Slope. Mar. Petrol. Geol. 28 (2), 427–438.
Dai, S., Santamarina, J.C., Waite, W.F., Kneafsey, T.J., 2012. Hydrate morphology: physical properties of sands with patchy hydrate saturation. J. Geophys. Res.: Solid Earth 117 (B11).
Dallimore, S.R., Yamamoto, K., Wright, J.F., Bellefleur, G., 2012. Scientific Results from the JOGMEC/NRCan/Aurora Mallik 2007-2008 Gas Hydrate Production Research Well Program, Mackenzie Delta, Northwest Territories. Geological Survey of Canada, Canada.
Dang, H., Luan, X.W., Chen, R., Zhang, X., Guo, L., Klotz, M.G., 2010. Diversity, abundance and distribution of amoA-encoding archaea in deep-sea methane seep sediments of the Okhotsk Sea. FEMS Microbiol. Ecol. 72 (3), 370–385.
Depreiter, D., Poort, J., Van Rensbergen, P., Henriet, J.P., 2005. Geophysical evidence of gas hydrates in shallow submarine mud volcanoes on the Moroccan margin. J. Geophys. Res.: Solid Earth 110 (B10).
Diaconescu, C.C., Knapp, J.H., 2002. Gas hydrates of the south caspian sea, Azerbaijan: drilling hazards and sea floor destabilizers. In: Offshore Technology Conference. Offshore Technology Conference.
Dillon, W.P., Popenoe, P., Grow, J.A., Klitgord, K.D., Swift, B.A., Paull, C.K., Cashman, K.V., 1982. Growth Faulting and Salt Diapirism: Their Relationship and Control in the Carolina Trough, Eastern North America: Rifted Margins: Field Investigations of Margin Structure and Stratigraphy. US Geological Survey. Woods Hole, Massachussets.
Exon, N.F., Dickens, G.R., Auzende, J.M., Lafoy, Y., Symonds, P.A., Van de Beuque, S., 1998. Gas hydrates and free gas on the lord Howe rise, tasman sea. PESA J. 26, 148–159.
Expedition 311 Scientists, 2005. Cascadia margin gas hydrates. IODP Prel. Rept. 311 10:2204/iodp.pr.311.2005.
Gardner, J.M., 2001. Mud volcanoes revealed and sampled on the Western Moroccan continental margin. Geophys. Res. Lett. 28 (2), 339–342.
Gay, A., Lopez, M., Berndt, C., Seranne, M., 2007. Geological controls on focused fluid flow associated with seafloor seeps in the Lower Congo Basin. Mar. Geol. 244 (1–4), 68–92.
Geletti, R., Busetti, M., 2011. A double bottom simulating reflector in the western Ross Sea, Antarctica. J. Geophys. Res.: Solid Earth 116 (B4).
Ginsburg, G.D., Milkov, A.V., Soloviev, V.A., Egorov, A.V., Cherkashev, G.A., Vogt, P.R., Crane, K., Lorenson, T.D., Khutorskoy, M.D., 1999. Gas hydrate accumulation at the Haakon Mosby mud volcano. Geo Mar. Lett. 19 (1–2), 57–67.
Ginsburg, G.D., Guseynov, R.A., Dadashev, A.A., Ivanova, G.A., Kazantsev, S.A., Solov'yev, V.A., Telepnev, E.V., Askeri-Nasirov, R.Y., Yesikov, A.D., Mal'tseva, V.I., Mashirov, Y.G., 1992. Gas hydrates of the southern Caspian. Int. Geol. Rev. 34 (8), 765–782.
Gregory, A.S., Whalley, W.R., Watts, C.W., Bird, N.R.A., Hallett, P.D., Whitmore, A.P., 2006. Calculation of the compression index and precompression stress from soil compression test data. Soil Tillage Res. 89 (1), 45–57.
Hayes, D.E., Shipboard Scientific Party, 1975. Site 273. Proc. Deep Sea Drill. Project 28, 335–367 Initial Reports.
Hollister, C.D., Shipboard Scientific Party, 1972. Site 107 – upper continental rise. Proc. Deep Sea Drill. Project 11, 351–356 Initial Reports.
Hovland, M., Lysne, D., Whiticar, M., 1995. Gas hydrate and sediment gas composition, Hole 892A. In: Proceedings of the Ocean Drilling Program, Scientific Results, vol. 146. pp. 151–162.
Hovland, M., Gallagher, J.W., Clennell, M.B., Lekvam, K., 1997. Gas hydrate and free gas volumes in marine sediments: example from the Niger Delta front. Mar. Petrol. Geol. 14 (3), 245–255.
Hustoft, S., Bünz, S., Mienert, J., Chand, S., 2009. Gas hydrate reservoir and active methane-venting province in sediments on < 20 Ma young oceanic crust in the Fram Strait, offshore NW-Svalbard. Earth Planet Sci. Lett. 284 (1–2), 12–24.
Jang, J., Santamarina, J.C., 2016. Fines classification based on sensitivity to pore-fluid chemistry. J. Geotech. Geoenviron. Eng. 10, 06015018 1061/(ASCE)GT.1943-5606.0001420.
Jang, J., Santamarina, J.C., 2017. Closure to "Fines classification based on sensitivity to pore-fluid chemistry" by Junbong Jang and J. Carlos Santamarina. J. Geotech. Geoenviron. Eng. 10, 07017013 1061/(ASCE)GT.1943-5606.0001694.
Jansen, E., Shipboard Scientific Party, 1996. Site 986. In: Proceedings of the Ocean Drilling Program, vol. 162. pp. 287–343 Initial Reports.
Judge, A., Smith, S.L., Majorowicz, J., 1994. January). The current distribution and thermal stability of natural gas hydrates in the Canadian Polar Regions. In: The Fourth International Offshore and Polar Engineering Conference. International Society of Offshore and Polar Engineers.
Kataoka, S., Yamashita, S., Kawaguchi, T., Suzuki, T., 2009. The soil properties of lake-bottom sediments in the Lake Baikal gas hydrate province. Soils Found. 49 (5), 757–775.
Kennet, J.P., Shipboard Scientific Party, 1986. Site 588: lord Howe rise, 26N. In: Proceedings of the Deep Sea Drilling Project, vol. 90. pp. 139–252.
Kenyon, N.H., Ivanov, M.K., Akhmetzhanov, A.M., Akhmanov, G.G., 2000. Multidisciplinary Study of Geological Processes on the North East Atlantic and Western Mediterranean Margins. IOC Technical Series, vol. 56 UNESCO.
Khlystov, O., De Batist, M., Shoji, H., Hachikubo, A., Nishio, S., Naudts, L., Poort, J., Khabuev, A., Belousov, O., Manakov, A., Kalmychkov, G., 2013. Gas hydrate of lake baikal: Discovery and varieties. J. Asian Earth Sci. 62, 162–166.
Kim, G.Y., Yi, B.Y., Yoo, D.G., Ryu, B.J., Riedel, M., 2011. Evidence of gas hydrate from downhole logging data in the Ulleung Basin, East Sea. Mar. Petrol. Geol. 28 (10), 1979–1985.
Kopp, H., 2002. BSR occurrence along the Sunda margin: evidence from seismic data. Earth Planet Sci. Lett. 197 (3–4), 225–235.
Kvenvolden, K.A., Barnard, L.A., 1983. Gas hydrate of the blake outer ridge, site 533, Deep Sea drilling project leg 76. In: Proceedings of the Ocean Drilling Program, vol. 76. pp. 353–365 Initial Reports.
Kvenvolden, K.A., McDonald, T.J., 1985. Gas hydrates of the Middle America trench—deep sea drilling project leg 84. Initial Reports of DSDP. 84. pp. 667–682.
Kvenvolden, K.A., Golan-Bac, M., Rapp, J.B., 1987. Hydrocarbon geochemistry of sediments offshore from Antarctica: wilkes Land continental margin. CPCEMR Earth Sci. Series 5A, 205–213.
Kvenvolden, K.A., Golan-Bac, M., McDonald, T.J., Pflaum, R.C., Brooks, J.M., 1989. Hydrocarbon gases in sediment of the voring plateau, Norwegian sea. In: Proceedings of the Ocean Drilling Program, Scientific Results, vol. 104. pp. 319–326.
Kvenvolden, K.A., Kastner, M., 1990. Gas hydrates of the peruvian outer continental margin. In: Proceedings of the Ocean Drilling Program, Scientific Results, vol. 112. pp. 517–526.
Ladd, J., Westbrook, G., Lewis, S., 1981. Subduction tectonics in forearcs: Guatemala vs. Barbados. Lamont-Doherty Geol. Observ. Yearbook 8 (2), 17–22.
Lee, C., Yun, T.S., Lee, J.S., Bahk, J.J., Santamarina, J.C., 2011. Geotechnical characterization of marine sediments in the ulleung basin, East sea. Eng. Geol. 117 (1–2), 151–158.
Lei, L., Santamarina, J.C., 2019. Physical properties of fine-grained sediments with segregated hydrate lenses. Mar. Petrol. Geol. 109, 899–911.
Lin, C.C., Lin, A.T.S., Liu, C.S., Chen, G.Y., Liao, W.Z., Schnurle, P., 2009. Geological controls on BSR occurrences in the incipient arc-continent collision zone off southwest Taiwan. Mar. Petrol. Geol. 26 (7), 1118–1131.
Liu, C., Meng, Q., He, X., Li, C., Ye, Y., Zhang, G., Liang, J., 2015. Characterization of natural gas hydrate recovered from pearl river mouth basin in south China sea. Mar. Petrol. Geol. 61, 14–21.
Lonsdale, M.J., 1990. The relationship between silica diagenesis, methane, and seismic reflections on the South Orkney microcontinent. In: Proceedings of the Ocean Drilling Program, Scientific Results, vol. 113. pp. 27–37.
Lu, Z., Zhu, Y., Zhang, Y., Wen, H., Li, Y., Liu, C., 2011. Gas hydrate occurrences in the Qilian Mountain permafrost, Qinghai province, China. Cold Reg. Sci. Technol. 66 (2–3), 93–104.
Luan, X., Jin, Y., Obzhirov, A., Yue, B., 2008. Characteristics of shallow gas hydrate in Okhotsk Sea. Sci. China Earth Sci. 51 (3), 415–421.
Lüdmann, T., Wong, H., 2003. Characteristics of gas hydrate occurrences associated with mud diapirism and gas escape structures in the northwestern Sea of Okhotsk. Mar. Geol. **201** (4), 269–286.
Lykousis, V., Alexandri, S., Woodside, J., De Lange, G., Dählmann, A., Perissoratis, C., Heeschen, K., Ioakim, C., Sakellariou, D., Nomikou, P., Rousakis, G., 2009. Mud volcanoes and gas hydrates in the anaximander mountains (eastern mediterranean sea). Mar. Petrol. Geol. 26 (6), 854–872.
Majorowicz, J.A., Hannigan, P.K., Osadetz, K.G., 2002. Study of the natural gas hydrate "Trap Zone" and the methane hydrate potential in the Sverdrup Basin, Canada. Nat. Resour. Res. 11 (2), 79–96.
Manley, P.L., Flood, R.D., 1989. Anomalous sound velocities in near-surface, organic-rich, gassy sediments in the central Argentine Basin. Deep Sea Research Part A. Oceanogr. Res. Pap. 36 (4), 611–623.
Manley, P.L., Flood, R.D., 1988. Cyclic sediment deposition within Amazon deep-sea fan. AAPG (Am. Assoc. Pet. Geol.) Bull. 72 (8), 912–925.
Manley, P.L., Pirmez, C., Busch, W., Cramp, A., 1997. Grain-size characterization of Amazon Fan deposits and comparison to seismic facies units. In: Proceedings of the Ocean Drilling Program. Scientific Results, pp. 35–52.
Matsumoto, R., Uchida, T., Waseda, A., Uchida, T., Takeya, S., Hirano, T., Yamada, K., Maeda, Y., Okui, T., 2000. Occurrence, structure, and composition of natural gas hydrate recovered from the Blake Ridge, Northwest Atlantic. In: Proceedings of the Ocean Drilling Program, Scientific Results, vol. 164. pp. 13–28.
Mayer, L.A., 1982. Physical properties of sediment recovered on Deep Sea Drilling Project Leg 68 with the hydraulic piston corer. Proc. Deep Sea Drill. Project 68, 365–382.
Mazurenko, L.L., Soloviev, V.A., Belenkaya, I., Ivanov, M.K., Pinheiro, L.M., 2002. Mud volcano gas hydrates in the Gulf of Cadiz. Terra. Nova 14 (5), 321–329.
McManus, D.A., Shipboard Scientific Party, 1969a. Introduction leg 5. In: Proceedings of the Deep Sea Drilling Project. vol. 5. pp. 3–14 Initial Reports.
McManus, D.A., Shipboard Scientific Party, 1969b. Site 35. In: Proceedings of the Deep Sea Drilling Project, vol. 5. pp. 165–202 Initial Reports.
Minshull, T.A., Singh, S.C., Westbrook, G.K., 1994. Seismic velocity structure at a gas hydrate reflector, offshore western Colombia, from full waveform inversion. J. Geophys. Res.: Solid Earth 99 (B3), 4715–4734.
Moore, J.C., Shipboard Scientific Party, 1982. Site 491. In: Proceedings of the Deep Sea Drilling Project, vol. 66. pp. 219–287 Initial Reports.
Moridis, G.J., 2008. Toward Production from Gas Hydrates: Current Status, Assessment of Resources, and Simulation-Based Evaluation of Technology and Potential. Lawrence Berkeley National Laboratory.
Moridis, G.J., Kowalsky, M.B., Pruess, K., 2007. Depressurization-induced gas production from class-1 hydrate deposits. SPE Reservoir Eval. Eng. 10 (5), 458–481.
Moridis, G.J., Silpngarmlert, S., Reagan, M.T., Collett, T., Zhang, K., 2011a. Gas production from a cold, stratigraphically-bounded gas hydrate deposit at the mount elbert gas hydrate stratigraphic test well, Alaska north slope: implications of uncertainties. Mar. Petrol. Geol. 28 (2), 517–534.
Moridis, G.J., Collett, T.S., Pooladi-Darvish, M., Hancock, S., Santamarina, C., Boswell, R.,

Kneafsey, T., Rutqvist, J., Kowalsky, M., Reagan, M.T., Sloan, E.D., 2011b. Challenges, Uncertainties and Issues Facing Gas Production from Gas Hydrate Deposits (No. LBNL-4254E). Lawrence Berkeley National Lab. (LBNL), Berkeley, CA (United States).
Mosher, D.C., 2011. A margin-wide BSR gas hydrate assessment: Canada's Atlantic margin. Mar. Petrol. Geol. 28 (8), 1540–1553.
Oliveira, S., Vilhena, O., Da Costa, E., 2010. Time–frequency spectral signature of Pelotas Basin deep water gas hydrates system. Mar. Geophys. Res. 31 (1–2), 89–97.
Parlaktuna, M., Erdogmus, T., 2001. Natural gas hydrate potential of the Black Sea. Energy Sources 23, 203–211.
Park, J., Santamarina, J.C., 2017. Revised soil classification system for coarse-fine mixtures. J. Geotech. Geoenviron. Eng. 143 (8), 04017039.
Park, J., Castro, G.M., Carlos Santamarina, J., 2018. Closure to "revised soil classification system for coarse-fine mixtures" by junghee Park and J. Carlos Santamarina. J. Geotech. Geoenviron. Eng. 144 (8), 07018019.
Paull, C.K., Shipboard Scientific Party, 1996a. Site 997. In: Proceedings of the Ocean Drilling Program. vol. 164. pp. 277–334 Initial Reports.
Paull, C.K., Shipboard Scientific Party, 1996b. Site 997. Initial Reports In: Proceedings of the Ocean Drilling Program. vol. 164 617-613.
Paull, C.K., Shipboard Scientific Party, 1996c. Site 995. In: Proceedings of the Ocean Drilling Program. vol. 164. pp. 611–620 Initial Reports.
Paull, C.K., Shipboard Scientific Party, 1996d. Site 991. In: Proceedings of the Ocean Drilling Program. vol. 164. pp. 599 Initial Reports.
Pecher, I.A., Barnes, P.M., LeVay, L.J., Expedition 372 Scientists, 2018. International Ocean Discovery Program, Expedition 372 Preliminary Report. International Ocean Discovery Program, pp. 1–35.
Pflaum, R.C., Brooks, J.M., Cox, H.B., Kennicutt II, M.C., Sheu, D.D., 1986. Molecular and isotopic analysis of core gases and gas hydrates, deep sea drilling project Leg 96. Initial Reports of the Deep Sea Drilling Project. 96. pp. 781–784.
Piper, D.J.W., Pirmez, C., Manley, P.L., Long, D., Flood, R.D., Normark, W.R., Showers, W., 1997. Mass-transport deposits of the amazon fan. In: Proceedings of the Ocean Drilling Program, Scientific Results, vol. 155. pp. 109–146.
Pittinger, A., 1989. The influence of biogenic silica on the geotechnical stratigraphy of the Voring Plateau, Norwegian Sea. In: Proceedings of the Ocean Drilling Program, Scientific Results, vol. 104. pp. 923–940.
Popescu, I., De Batist, M., Lericolais, G., Nouzé, H., Poort, J., Panin, N., Versteeg, W., Gillet, H., 2006. Multiple bottom-simulating reflections in the Black Sea: potential proxies of past climate conditions. Mar. Geol. 227 (3–4), 163–176.
Reed, D.L., Silver, E.A., Tagudin, J.E., Shipley, T.H., Vrolijk, P., 1990. Relations between mud volcanoes, thrust deformation, slope sedimentation, and gas hydrate, offshore north Panama. Mar. Petrol. Geol. 7 (1), 44–54.
Ren, X.W., Santamarina, J.C., 2018. The hydraulic conductivity of sediments: a pore size perspective. Eng. Geol. 233, 48–54.
Ruppel, C.D., 2011. Methane hydrates and contemporary climate change. Nature Educ. Knowl 3 (10), 12.
Ruppel, C.D., Kessler, J.D., 2017. The interaction of climate change and methane hydrates. Rev. Geophys. 55, 126–168. https://doi.org/10.1002/2016RG000534.
Sættem, J., Poole, D.A.R., Ellingsen, L., Sejrup, H.P., 1992. Glacial geology of outer bjørnøyrenna, southwestern barents sea. Mar. Geol. 103 (1–3), 15–51.
Santa Ana, H., Latrónica, L., Tomasini, J., Morales, E., Ferro, S., Gristo, P., Machado, L., 2008. Economic and exploratory review of gas hydrates and other gas manifestations of the Uruguayan continental shelf. In: 6th International Conference of Gas Hydrates (ICGH 2008), (Vancouver, British Columbia, Canada).
Santamarina, J.C., Klein, K.A., Fam, M.A., 2001. Soils and Waves: Particulate Materials Behavior, Characterization and Process Monitoring. Wiley, Chichester, U.K.
Santamarina, J.C., Klein, K., Wang, D.S., Prencke, E., 2002. Specific surface: determination and relevance. Can. Geotech. J. 39 (1), 233–241.
Sarıtaş, H., Çifçi, G., Géli, L., Thomas, Y., Marsset, B., Henry, P., Grall, C., Rochat, A., 2018. Gas occurrence and shallow conduit systems in the Western Sea of Marmara: a review and new acoustic evidence. Geo Mar. Lett. 38 (5), 385–402.
Swart, R., 2009. Hydrate occurrences in the namibe basin, offshore Namibia. Geol. Soc. Lond. Special Pub. 319 (1), 73–80.
Sawyer, D.E., Jacoby, R., Flemings, P., Germaine, J.T., 2009. Data report: particle size analysis of sediments in the ursa basin, IODP expedition 308 sites U1324 and U1322, northern gulf of Mexico. In: Proc. IODP, vol. 308.
Schwalenberg, K., Haeckel, M., Poort, J., Jegen, M., 2010. Evaluation of gas hydrate deposits in an active seep area using marine controlled source electromagnetics: results from Opouawe Bank, Hikurangi Margin, New Zealand. Mar. Geol. 272 (1–4), 79–88.
Sheridan, R.E., Shipboard Scientific Party, 1980. Site 533 – blake outer ridge. Proc. Deep Sea Drill. Project 76, 35–140 Initial Reports.
Shin, H., Santamarina, J.C., 2017. Sediment–well interaction during depressurization. Acta Geotechnica 12 (4), 883–895.
Shipley, T.H., Houston, H.H., Buffler, R.T., 1979. Widespread occurrence of possible gas-hydrate horizons from continental slopes as identified on seismic reflection profiles. Proc. 11th Offshore Tech. Conf. 11 (3), 1879–1886.
Shoji, H., Minami, H., Hachikubo, A., Sakagami, H., Hyakutake, K., Soloviev, V., Matveeva, T., Mazurenko, L., Kaulio, V., Gladysch, V., Logvina, E., 2005. Hydrate-bearing structures in the sea of okhotsk. Eos, Trans. Am. Geophy. Union 86 (2), 13–18.
Suess, E., Shipboard Scientific Party, 1990. Site 688. Proc. Ocean Drill. Project 112, 873–1004 Initial Reports.
Sultan, N., Garziglia, S., Ruffine, L., 2016. New insights into the transport processes controlling the sulfate-methane-transition-zone near methane vents. Sci. Rep. 6.
Sun, Z., Santamarina, J.C., 2019. Haines jumps: pore scale mechanisms. Phys. Rev. E 100, 023115.
Tabatabaie, S.H., Pooladi-Darvish, M., 2009. Analytical solution for gas production from hydrate reservoirs underlain with free gas. J. Nat. Gas Sci. Eng. 1 (1–2), 46–57.
Tamaki, K., Pisciotto, K., Allan, J., et al., 1990. Site 796. Proc. Ocean Drill. Program 127, 247–322 Initial Reports.
Tamaki, K., Shipboard Scientific Party, 1990. Site 796. Proc. Ocean Drill. Program 127, 615–663 Initial Reports.
Tan, B., Germaine, J.T., Flemings, P.B., 2006. Data report: consolidation and strength characteristics of sediments from ODP Site 1244, Hydrate Ridge, Cascadia continental margin. Proc. Ocean Drill. Progr. Sci. Results 204, 1–148.
Talwani, M., Shipboard Scientific Party, 1976. Sites 338-343. Proc. Deep Sea Drill. Project 38, 151–387 Initial Reports.
Taylor, E., Bryant, W.R., 1985. Geotechnical properties of sediments from the Middle America Trench and slope. Initial Rep. Deep Sea Drill. Proj. 84, 745–766.
Terzariol, M., Goldsztein, G., Santamarina, J.C., 2017. Maximum recoverable gas from hydrate bearing sediments by depressurization. Energy 141, 1622–1628.
Tomasini, J., de Santa Ana, H., Conti, B., Ferro, S., Gristo, P., Marmisolle, J., et al., 2011. Assessment of marine gas hydrates and associated free gas distribution offshore Uruguay. J. Geol. Res. 1–7 2011.
Trimonis, E.S., Shimkus, K.M., 1978. Grain–size of the black sea sediments, DSDP leg 42B. Initial Reports of the Deep Sea Drilling Project. 42. pp. 427–450 2.
Tucholke, B.E., Bryan, G.M., Ewing, J.I., 1977. Gas-hydrate horizons detected in seismic-profiler data from the western North Atlantic. AAPG Bull. 61 (5), 698–707.
Uchida, T., Dallimore, S., Mikami, J.U.N., 2000. Occurrences of natural gas hydrates beneath the permafrost zone in Mackenzie Delta: visual and X-ray CT imagery. Ann. N. Y. Acad. Sci. 912 (1), 1021–1033.
Uchida, T., Lu, H., Tomaru, H., 2004. Subsurface occurrence of natural gas hydrate in the Nankai Trough area: implication for gas hydrate concentration. Resour. Geol. 54 (1), 35–44.
Uchida, T., Yamamoto, J., Okada, S., Waseda, A., Baba, K., Okatsu, K., R, Matsumoto, Shipboard Scientific Party, 1997. Methane hydrates in deep marine sediments X-ray CT and NMR studies of ODP Leg 164. J. Geol. Survey Jn. 510, 36–42.
Vallier, T.L., 1969. Grain size analysis. Leg 5. Proc. Deep Sea Drill. Project 5, 421–430.
von Lom-Keil, H., Spieß, V., Hopfauf, V., 2002. Fine-grained sediment waves on the western flank of the Zapiola Drift, Argentine Basin: evidence for variations in Late Quaternary bottom flow activity. Mar. Geol. 192 (1–3), 239–258.
Waite, W.F., Santamarina, J.C., Cortes, D.D., Dugan, B., Espinoza, D.N., Germaine, J., Jang, J., Jung, J.W., Kneafsey, T.J., Shin, H., Soga, K., 2009. Physical properties of hydrate-bearing sediments. Rev. Geophys. 47 (4), RG4003.
Wang, J., Wu, S., Kong, X., Li, Q., Wang, J., Ding, R., 2018. Geophysical characterization of a fine-grained gas hydrate reservoir in the Shenhu area, northern South China Sea: integration of seismic data and downhole logs. Mar. Petrol. Geol. 92, 895–903.
Wang, P., Zhu, Y., Lu, Z., Huang, X., Pang, S., Zhang, S., 2014a. Gas hydrate stability zone migration occurred in the Qilian Mountain permafrost, Qinghai, Northwest China: evidences from pyrite morphology and pyrite sulfur isotope. Cold Reg. Sci. Technol. 98, 8–17.
Wang, X., Collett, T.S., Lee, M.W., Yang, S., Guo, Y., Wu, S., 2014b. Geological controls on the occurrence of gas hydrate from core, downhole log, and seismic data in the Shenhu area, South China Sea. Mar. Geol. 357, 272–292.
Wang, X., Hutchinson, D.R., Wu, S., Yang, S., Guo, Y., 2011. Elevated gas hydrate saturation within silt and silty clay sediments in the Shenhu area, South China Sea. J. Geophys. Res.: Solid Earth 116 (B5).
Wang, Y., Feng, J.C., Li, X.S., Zhang, Y., Li, G., 2015. Analytic modeling and large-scale experimental study of mass and heat transfer during hydrate dissociation in sediment with different dissociation methods. Energy 90, 1931–1948.
Warren, L.P., Shipboard Scientific Party, 1979. Site 502 – Colombia basin, western caribbean sea. Proc. Deep Sea Drill. Project 68, 15–162 Initial Reports.
Weaver, J.S., Stewart, J.M., 1982. In situ hydrates under the Beaufort Sea shelf. Proceedings, Fourth Canadian Permafrost Conference. pp. 312–319.
Wefer, G., Shipboard Scientific Party, 1998a. Site 1076. In: Proceedings of the Ocean Drilling Program, vol. 175. pp. 87–113 Initial Reports.
Wefer, G., Shipboard Scientific Party, 1998b. Site 1080. In: Proceedings of the Ocean Drilling Program, vol. 175. pp. 201–221 Initial Reports.
Wei, J., Pape, T., Sultan, N., Colliat, J.L., Himmler, T., Ruffine, L., de Prunelé, A., Dennielou, B., Garziglia, S., Marsset, T., Peters, C.A., 2015. Gas hydrate distributions in sediments of pockmarks from the Nigerian margin–Results and interpretation from shallow drilling. Mar. Petrol. Geol. 59, 359–370.
Westbrook, G.K., Shipboard Scientific Party, 1994a. Leg 146 introduction: cascadia margin. Proc. Deep Sea Drill. Project 146, 5–14 Initial Reports.
Westbrook, G.K., Shipboard Scientific Party, 1994b. Sites 889 and 890. In: Proceedings of the Deep Sea Drilling Project, vol. 146. pp. 127–239 Initial Reports.
White, R.S., 1979. Gas hydrate layers trapping free gas in the Gulf of Oman. Earth Planet Sci. Lett. 42 (1), 114–120.
Whitmarsh, R.B., Shipboard Scientific Party, 1974. Site 222. In: Proceedings of the Deep Sea Drilling Project, vol. 23. pp. 211–289 Initial Reports.
Winters, W.J., 2000. Stress history and geotechnical properties of sediment from the cape fear diapir, blake ridge diapir, and blake ridge. In: Proceedings of the Ocean Drilling Program, Scientific Results, vol. 164. pp. 421–429.
Winters, W.J., Waite, W.F., Mason, D.H., Kumar, P., 2008. Physical properties of repressurized samples recovered during the 2006 national gas hydrate program expedition offshore India. In: 6th International Conference on Gas Hydrates, pp. 6–10 Chevron, Vancouver, BC, Canada.
Winters, W., Walker, M., Hunter, R., Collett, T., Boswell, R., Rose, K., Waite, W., Torres, M., Patil, S., Dandekar, A., 2011. Physical properties of sediment from the Mount Elbert gas hydrate stratigraphic test well, Alaska North Slope. Mar. Petrol. Geol. 28 (2), 361–380.
Yamamoto, K., Terao, Y., Fujii, T., Ikawa, T., Seki, M., Matsuzawa, M., Kanno, T., 2014.

May. Operational overview of the first offshore production test of methane hydrates in the Eastern Nankai Trough. In: Offshore Technology Conference. Offshore Technology Conference.
Yoneda, J., Masui, A., Konno, Y., Jin, Y., Egawa, K., Kida, M., Ito, T., Nagao, J., Tenma, N., 2015. Mechanical properties of hydrate-bearing turbidite reservoir in the first gas production test site of the Eastern Nankai Trough. Mar. Petrol. Geol. 66, 471–486.
Yun, T.S., Narsilio, G.A., Santamarina, J.C., 2006. Physical characterization of core samples recovered from Gulf of Mexico. Mar. Petrol. Geol. 23 (9–10), 893–900.
Yun, T.S., Santamarina, J.C., Ruppel, C., 2007. Mechanical properties of sand, silt, and clay containing tetrahydrofuran hydrate. J. Geophys. Res.: Solid Earth 112 (B4), B04106.
Yun, T.S., Fratta, D., Santamarina, J.C., 2010. Hydrate-bearing sediments from the Krishna − Godavari Basin: physical characterization, pressure core testing, and scaled production monitoring. Energy Fuel. 24 (11), 5972–5983.
Zhao, J., Yu, T., Song, Y., Liu, D., Liu, W., Liu, Y., Yang, M., Ruan, X., Li, Y., 2013. Numerical simulation of gas production from hydrate deposits using a single vertical well by depressurization in the Qilian Mountain permafrost, Qinghai-Tibet Plateau, China. Energy 52, 308–319.